Published in final edited form as:
Bioconjug Chem. 2013 June 19; 24(6): 897–906. doi:10.1021/bc300592d.

Inducing Cancer Cell Death by Targeting its Nucleus: Solid Gold Nanospheres versus Hollow Gold Nanocages

Megan A. Mackey, **Farhat Saira**, **Mahmoud A. Mahmoud**, and **Mostafa A. El-Sayed***
Laser Dynamics Laboratory, School of Chemistry and Biochemistry, Georgia Institute of Technology, Atlanta, Georgia, USA

Abstract

Recently, we have shown that targeting the cancer cell nucleus with solid gold nanospheres, using a cancer cell penetrating/pro-apoptotic peptide (RGD) and a nuclear localization sequence peptide (NLS), inhibits cell division, thus leading to apoptosis. In the present work, flow cytometric analysis revealed an increase in cell death, via apoptosis and necrosis, in HSC cells upon treatment with peptide-conjugated hollow gold nanocages, compared to those treated with the peptide-conjugated solid gold nanospheres. This is consistent with a G0/G1 phase accumulation, S phase depletion and G2/M phase depletion, as well as reduced ATP levels. Here, we investigate the possible causes for the observed enhanced cell death with the use of confocal microscopy. The fluorescence images of HSC cells treated with gold nanocages, indicate the presence of reactive oxygen species, known to cause apoptosis. The formation of reactive oxygen species observed is consistent with a mechanism involving the oxidation of metallic silver on the inner cavity of the nanocage (inherent to the synthesis of the gold nanocages), to silver oxide. This oxidation is confirmed by an observed redshift in the surface plasmon resonance of the gold nanocages in cell culture medium. The silver oxide, a semiconductor known to photochemically generate hydroxyl radicals, a form of reactive oxygen species, is proposed as a mechanism for the enhanced cell death caused by gold nanocages. Thus, the enhanced cell death, via apoptosis and necrosis, observed with peptide-conjugated hollow gold nanocage-treated cells is considered to be a result of the metallic composition (silver remaining on the inner cavity) of the nanocage.

INTRODUCTION

Gold nanostructures and their interactions with biological systems are growing increasingly important, especially in biomedical research. Due to their unique optical properties, gold nanoparticles exhibit extrinsic activation as photothermal contrast agents, ultimately enabling the photothermal ablation of tumors by use of core-shell nanoparticles,[1, 2] gold nanorods,[3-5] gold nanocages,[6] and spherical gold nanoparticles.[5, 7] As our group has recently demonstrated, using peptide-conjugated gold and silver nanoparticles to target cancer cells *in vitro*,[8, 9] nanostructures also exhibit intrinsic antineoplastic capabilities. These targeted nanoparticles not only cause changes in the cell cycle and induce apoptosis, but their location in the cell can also be determined using plasmonic imaging, due to their high scattering cross-section, as was first demonstrated by El-Sayed and coworkers.[10] By utilizing polyethylene glycol (PEG) to minimize non-specific uptake, as well as an RGD

*Corresponding author: 901 Atlantic Drive, Atlanta, Georgia, 30332-0400, USA. phone: 404-894-0292, fax: 404-894-7452, melsayed@gatech.edu.

Supporting Information Available: Zeta potential measurements, confocal microscopy images showing nanoparticle-nucleus co-localization, additional HSC cell cycle analysis and histograms, HSC apoptosis and necrosis measurements, confocal images of ROS generation in HSC cells for other nanoparticle formulations tested, and apoptosis and necrosis measurements for control cell line (HaCat) are provided. This material is free of charge via the Internet at http://pubs.acs.org.

(arginine-glycine-aspartic acid) sequence peptide and an NLS (nuclear localization sequence) peptide, nanoparticles are targeted to alpha v beta integrins on the cancer cell surface[11-14] and translocated to the nuclear pore complex,[15-17] respectively. Not only does the RGD peptide target integrins on the cell surface to serve as a cell penetration peptide, but it has also been characterized as a pro-apoptotic peptide, which induces rapid autoprocessing of the caspase-3 proenzyme, via interactions with an RGD-binding motif, causing subsequent caspase-3 activation.[18, 19] Previous reports of RGD and NLS peptides having the ability to target gold nanoparticles to the nucleus of cancer cells,[16, 20, 21] as well as the extensive studies done on the fundamental and applied properties of gold nanocages,[6, 22-25] provide an excellent platform for further investigation of the antineoplastic properties of gold nanostructures, both solid gold nanospheres and hollow gold nanocages. One such property exhibited by gold nanostructures is the ability to modulate the cell cycle in malignant cells, which have characteristic sensitivities to cell cycle disruption, and, due to inherently compromised repair mechanisms, malignant cells can undergo subsequent apoptosis.[8, 9]

In the present work, we compare the efficacy at which nuclear-targeting gold nanostructures, of different shapes, induce disruptions in the cellular functions of HSC (human oral squamous carcinoma) cells. We specifically detect cell cycle disruptions, ATP depletion, and apoptotic and necrotic cell populations induced by both solid gold nanospheres and hollow gold nanocages. We found that the gold nanocages are much more effective in disrupting cellular functions and causing cell death than the gold nanospheres. This is shown to result from the presence of reactive oxygen species (ROS) species, known to cause apoptosis in living cells.[26] From our previous work using gold nanocages for the destruction of pollutant azo dyes,[25] we concluded that the silver remaining on the inner cavity of the gold nanocages, inherent to their synthesis, is photochemically oxidized to silver oxide, which produces reactive oxygen species. Therefore, the different metallic compositions are proposed to be the cause of different cellular disruptions observed between the nanospheres and nanocages.

EXPERIMENTAL PROCEDURES

Cell culture

Human oral squamous cell carcinoma (HSC-3) cells were maintained in Dulbecco's modified Eagle's medium (DMEM, Mediatech) supplemented with 10% v/v fetal bovine serum (FBS, Mediatech) and 1% v/v antimycotic solution (Mediatech) in a 37°C, 5% CO_2 humidified incubator.

Nanoparticle synthesis and peptide conjugation

Gold nanocages (AuNCs), with a 45 nm wall length and a 5 nm wall thickness, were prepared via galvanic replacement reaction with silver nanocubes as a template.[22] Silver nanocubes were prepared by a previously reported method.[24] Briefly, 70 mL of ethylene glycol (EG) was heated to 150°C for 1 h, followed by the addition of polyvinyl pyrrolidone (PVP, MW 55,000; 0.82 g dissolved in 5 mL EG). While still at 150°C, 0.7 mL of a 3 mM sodium sulfide solution (in EG) was added, followed by slow injection of 4 mL of a silver nitrate solution (0.48 g dissolved in 10 mL EG). [25, 27] The reaction was allowed to proceed to completion (10-15 min) resulting in the reduction of silver ions to silver nanocubes. The silver nanocubes were purified by adding a 1:2 acetone/water mixture at a volume two times that of the nanocube solution, centrifuging at 14,000 rpm for 5 min and redispersing the precipitate in 200 mL of water. The silver nanocube solution was brought to a boil under reflux, after which a 10 mg/L hydrogen tetrachloroaurate ($HAuCl_4$) solution was slowly injected and the UV-Vis spectrum of the solution was monitored until the absorption

maximum red-shifted and remained constant at about 720 nm.[27] The AuNCs were then purified by centrifugation at 14,000 rpm for 5 min and redispersed in water. The surface plasmon absorption spectrum of the PVP-AuNCs can be found in Fig. 1A (black). Transmission electron microscopy (TEM) reveals the AuNCs synthesized here are between 40 and 50 nm in wall length (Fig. 1C).

Gold nanospheres (AuNSs), with a 35 nm diameter, were synthesized based on the method developed by Frens.[28] Briefly, 20 mL of a 1 mM $HAuCl_4$ solution was brought to a boil, under reflux, while stirring, followed by addition of 0.5 mL of a 1% trisodium citrate solution. Reaction completion was determined by the color changing from clear to a deep red/purple. The UV-Vis spectrum of the solution showed the absorption maximum to be around 535 nm for the AuNSs. The AuNSs were then purified by centrifugation at 6000 rpm for 15 min and redispersed in water. The surface plasmon absorption spectrum of the citrate-AuNSs can be found in Fig. 1B (black). Transmission electron microscopy (TEM) reveals the AuNSs synthesized here are between 30 and 40 nm in diameter (Fig. 1D).

Prior to peptide conjugation, the AuNCs and AuNSs were coated with thiol-terminated polyethylene glycol (mPEG-SH 5000) through a Au-S bond. This was done in order to prevent nonspecific adsorption of proteins to the particles in a physiological environment. A 1 mM aqueous solution of PEG was added to AuNPs at 10^4 molar excess, and left overnight. Particles were then purified by centrifugation at 6000 rpm for 15 min and resuspended in water. The surface plasmon absorption spectrum of the PEG-AuNCs and PEG-AuNSs can be found in Fig. 1A,B (red), respectively.

After PEGylation the AuNCs and AuNSs were further conjugated with custom peptides purchased from GenScript USA, Inc. Specifically, an RGD (RGDRGDRGDRGDPGC) peptide and an NLS (CGGGPKKKRKVGG) peptide, both with C-terminal amidation, were used in this work. Conjugation of peptides was achieved by addition of a 5 mM aqueous solution of peptide to the PEG coated nanoparticles at 1×10^4 molar excess of NLS peptides/nanoparticle and 8×10^3 molar excess of RGD peptides/nanoparticle for 24 h, after which the peptide conjugated nanoparticles were centrifuged at 6000 rpm for 15 min and redispersed in water to render RGD-AuNCs, RGD-AuNSs, NLS-AuNCs, NLS-AuNSs, RGD/NLS-AuNCs, and RGD/NLS-AuNCs. The hydrodynamic diameter of the peptide-conjugated gold nanoparticles was determined using dynamic light scattering (DLS). The hydrodynamic diameter of the PEG-conjugated and peptide-conjugated AuNSs and AuNCs is drastically different although the actual gold nanoparticle size varies only by 10 nm. Upon conjugation with PEG, and RGD and NLS peptides, the hydrodynamic diameter of AuNCs increases to 96 nm while the RGD/NLS-AuNSs have a hydrodynamic diameter of 42 nm. The size increase to almost 100 nm observed in the case of the conjugated AuNCs is in agreement with the hydrodynamic diameter measurements previously observed, by Xia and coworkers[29], for PEG conjugated AuNCs. Further confirmation that the nanoparticle surface was modified during conjugation of PEG and peptides was achieved through zeta potential measurements, shown in Table S1.

The peptide conjugated AuNCs and AuNSs were further diluted in DMEM to 0.1 and 0.4 nM, for treatment of HSC-3 cells. The gold nanoparticle concentrations were determined using $\varepsilon = 5.0\times10^9$ (AuNCs), which was calculated based on ICP measurements, and $\varepsilon = 5.3\times10^9$ (AuNSs), which is based on previous reports.[30]

Gold nanoparticle internalization

Two different methods were used to determine nanoparticle uptake by HSC-3 cells. First, to determine the percentage of nanoparticles taken up by HSC-3 cells, a previously utilized spectroscopic method was used[9]. Specifically, the cells were grown in 96-well tissue culture

plates overnight. The growth media was then removed and replaced with growth media containing gold nanoparticles. After a 48 h incubation period with gold nanoparticles, the gold nanoparticle-containing media was removed and placed into a cell-free 96-well plate. The optical density was analyzed on a Biotek Synergy H4 multi-mode plate reader at wavelengths of 723 and 538 nm (plasmon absorption for the AuNCs and AuNSs, respectively). In order to determine nanoparticle uptake, the recorded optical density was subtracted from the optical density of the gold nanoparticle-containing growth media initially added to the cell culture. This value was then converted to a percentage of what was initially added to the cell culture. Second, to visualize the nanoparticles inside HSC-3 cells by plasmonic dark field light scattering imaging, cells were grown on coverslips for 24 h, after which the culture medium was removed and replaced with nanoparticle-containing medium. HSC-3 cells were then grown in the presence of 0.4 nM peptide-conjugated gold nanoparticles for 48 h. The nanoparticle-containing medium was removed and the cells were washed with PBS buffer. In order to remove nanoparticles that have not been internalized by the HSC-3 cells, a previously developed etching method was used.[31] Briefly, 1 mL of an aqueous solution containing a 1:6 molar ratio mixture of I_2 (0.34 mM) and KI was added to the cells and removed after 5 min. The coverslips were then washed with deionized water. The cells were then fixed with 4% paraformaldehyde. Dark field images were taken using an inverted Olympus IX70 microscope utilizing a dark field condenser (U-DCW) and a 100x/1.35 oil Iris objective (UPLANAPO).

Flow cytometry cell cycle analysis

HSC-3 cells were grown in 12-well tissue culture plates overnight. The growth media was then removed and replaced with growth media containing gold nanoparticles. After cells were treated with gold nanoparticles for 48 h, they were fixed in 70% ethanol, centrifuged, washed, and resuspended in phosphate buffered saline (PBS). Cells were then treated with 10 μg/mL RNase (Sigma) at 37°C for 30 min, after which they were stained with 100 μg/mL of propidium iodide (PI), fluorescent DNA stain, for 15 min at room temperature. Samples, consisting of 10,000 cells, in triplicate, were analyzed using the BD LSR II (BD Biosciences) with a 488 nm excitation. Using the flow cytometry analysis software, FlowJo, DNA content and subsequent cell cycle analyses were carried out.

ATP assay

HSC-3 cells were grown in white opaque-walled 96-well tissue culture plates overnight, after which the growth media was replaced with gold nanoparticle-containing media. Upon 48 h treatment with nanoparticles, the CellTiter-Glo® Luminescent Cell Viability Assay was used according to the manufacturer's protocol. Briefly, the CellTiter-Glo® Reagent was prepared by mixing the CellTiter-Glow® Buffer with the CellTiter-Glo® Substrate. After 48 h gold nanoparticle treatment, the cells were rinsed with PBS, 100 μL of fresh media was added, and the plate was allowed to equilibrate to room temperature. 100 μL of the CellTiter-Glo® Reagent was then added to the cells and the plate was mixed on an orbital shaker for 2 min to promote cell lysis. Luminescence was then recorded on a Biotek Synergy H4 multi-mode plate reader. This method provides a quantitative measurement of the amount of ATP in the cell culture, and can be used as a cell viability assay, as the luminescence signal is directly correlated to the number of metabolically active cells, based on their ATP production.[32]

Flow cytometry analysis of apoptosis and necrosis

HSC-3 cells were grown in 12-well tissue culture plates overnight, after which the growth media was removed and replaced with growth media containing gold nanoparticles. After cells were treated with gold nanoparticles for 48 h, an Alexa Fluor 488 annexin-V/Dead Cell Apoptosis kit for flow cytometry (Invitrogen) was used for the detection of apoptosis and

necrosis. The standard protocol was optimized for our experimental conditions. Briefly, cells were centrifuged, washed, and resuspended in 1 mL of 1X annexin-binding buffer. After which 5 μL of Alexa Fluor 488 annexin-V and 2 μL of 100 mg/mL propidium iodide (PI) were added to the cell suspension and left to incubate at room temperature for 15 min. Upon completion of dye loading, 1 mL of 1X annexin-binding buffer was added. Cells were analyzed immediately using the BD LSR II (BD Biosciences) with a 488 nm excitation on 10,000 cells, in triplicate. Using the flow cytometry analysis software, FlowJo, the Alexa Fluor 488 and PI intensities were gated based on a negative control (HSC-3 cells in nanoparticle-free media) and a positive control for apoptosis (HSC-3 cells treated with 10 μM camptothecin for 4 h).

Confocal acquisition of ROS

HSC-3 cells were grown on coverslips overnight. The growth media was then removed and replaced with growth media containing gold nanoparticles. After a 24 h incubation period with gold nanoparticles, the gold nanoparticle-containing media was removed and the cells were washed with PBS, after which the cells were stained with a 10 μM solution of H2DCFDA (6-carboxy-2′,7′-dichlorodihydrofluorescein diacetate, Invitrogen, C2938) and left to incubate at 37°C for 30 min. After dye loading, the cells were washed with PBS and fixed with 4% paraformaldehyde for 15 min, followed by nuclear staining with DAPI (4′6-Diamidino-2-phenylindole, Dihydrochloride, Invitrogen) and washing with water. Fluorescence images were taken by multiphoton confocal microscopy using the Zeiss LSM 510 NLS META with 785 (DAPI) and 488 nm (FITC) excitation sources.

Statistical analysis

All results are expressed as the mean ± standard deviation of three independent experiments. Statistical significance (*i.e.* p-value) was calculated using a *t-test calculator* (GraphPad Software, Inc.) and the data is considered statistically significant (indicated by *) when $p < 0.05$.

RESULTS AND DISCUSSION

HSC cells were treated with gold nanoparticles of different shape: solid gold nanospheres (AuNSs, ~35 nm diameter) and hollow gold nanocages (AuNCs, ~45 nm wall length) as shown in Figure 1. These two distinctly shaped gold nanoparticles were stabilized with polyethylene glycol thiol (mPEG-SH, MW 5000) in order to prevent any nonspecific interactions that might take place with these nanoparticles in the physiological environment. The PEGylated gold nanoparticles were then functionalized with specific peptides: an RGD (arginine-glycine-aspartic acid) sequence peptide and an NLS (nuclear localization sequence) peptide. The RGD peptide provides for receptor-mediated uptake of nanoparticles by cancer cells, as it mimics extracellular matrix proteins and targets alpha v beta integrins that are overexpressed on the cell surface of HSC cells,[12, 33] while also exhibiting pro-apoptotic capabilities.[18, 19] The NLS peptide from the simian virus (SV) large T antigen, having a KKKRK (lysine-lysine-lysine-arginine-lysine) sequence, provides for nuclear localization of nanoparticles, by binding importin alpha in the cytoplasm of the cell, which subsequently binds importin beta located on the cytoplasmic side of the nuclear membrane.[34-38] Peptide conjugation was exploited to give rise to six different types of gold nanoparticles, RGD-AuNSs NLS-AuNSs, RGD/NLS-AuNSs, RGD-AuNCs, NLS-AuNCs, and RGD/NLS-AuNCs. Each nanoparticle type exhibited cellular internalization, with the NLS peptide-conjugated nanoparticles showing subsequent nuclear localization. Cellular internalization (*i.e.* nanoparticle uptake) is shown in Figure 2A. Overall, each nanoparticle formulation exhibits about 50% uptake by HSC cells over 48 h. In order to confirm the internalization of the nanoparticles, plasmonic dark field imaging and a previously

developed etching technique were employed.[31] With this technique, it can be seen that the plasmonic dark field light scattering images, before and after the removal of extracellular nanoparticles by I_2/KI etching, are the same, suggesting nanoparticle internalization by HSC cells has occurred. Also, these images suggest the nuclear localization of the nanoparticles conjugated with the NLS peptide, while those without appear to be more dispersed throughout the cytoplasm of the cell, as we have shown previously with similar nanoparticle formulations.[8] Co-localization of the RGD/NLS-AuNSs and RGD/NLS-AuNCs with the nucleus was also confirmed with confocal imaging (see Figure S1 in Supporting Information for details). Upon confirmation of nuclear and cytoplasmic localization, all nanoparticles were examined in terms of their effects on HSC cellular functions, as well as their ability to induce cell death via apoptosis and necrosis.

Nanoparticle-induced disruption of cellular functions

Cell cycle analysis was utilized in order to compare the dependence of cell cycle disruption on nanoparticle shape (solid sphere or hollow cage), as well as nanoparticle concentration (0.1 or 0.4 nM). The most significant changes seen for all of the nanoparticle formulations occur when HSC cells are treated with a 0.4 nM concentration. With this high concentration, HSC cells experience cell cycle disruptions that have been previously linked to apoptosis.[39] The cell cycle changes observed for the RGD/NLS-AuNSs and RGD/NLS-AuNCs, as shown in Figure 3 (A and B, respectively), are an increased G0/G1 phase population (16% by AuNCs and 19% by AuNSs), a decreased S phase population (10% by AuNCs and 2% by AuNSs) and a decreased G2/M phase population (100% by both AuNCs and AuNSs). Similar trends are seen with the RGD-conjugated and NLS-conjugated gold nanoparticles (see Figure S2) except when HSC cells are treated with 0.1 nM RGD-AuNCs. In this case, a prominent G2/M arrest is observed, which has been correlated to cytokinesis arrest and apoptosis.[8] The more common trend observed here, G0/G1 phase accumulation and subsequent S phase depletion, has been attributed to a decrease in cellular ATP, as demonstrated using mitochondrial function disrupting agents.[40] Therefore, a direct quantitative measure of the ATP in gold nanoparticle-treated HSC cells was carried out. As shown in Figure 4, the amount of ATP present in cells is reduced with increased nanoparticle treatment concentrations for all nanoparticle formulations. The greatest reduction in ATP is observed with 0.4 nM RGD/NLS-AuNCs and RGD/NLS-AuNSs, as would be expected, based on the cell cycle changes observed for these two nanoparticle treatments (Fig. 3C and 3D). When HSC cells are treated with 0.4 nM RGD/NLS-AuNCs, ATP production is reduced to about 38%, which is slightly lower than the 43% ATP production observed with 0.4 nM RGD/NLS-AuNS-treated cells. With previous evidence of the reduction of ATP leading to apoptosis[39], the sub G1 cell population observed in the cell cycle histograms (Figure S3), and the efficacy at which these HSC cell nucleus targeting (RGD/NLS) nanoparticles reduce ATP in HSC cells, it is imperative to assess the fate of these physiological changes and to determine if the outcome (*i.e.* apoptosis and/or necrosis) is dependent on the nanoparticle structure (*i.e.* solid sphere vs. hollow cage). In order to directly resolve whether or not the peptide-conjugated gold nanoparticles utilized in this study cause apoptosis and/or necrosis, flow cytometric analysis of Alexa Fluor 488 conjugated annexin-V and propidium iodide (PI) in HSC cells was utilized. One of the earliest events that take place during apoptosis is the exposure of phosphatidylserine (PS) residues on the outer leaflet of the cell membrane. These PS residues have a high affinity for the phospholipid binding protein annexin-V. Therefore, by exposing cells to fluorescently labeled annexin-V, apoptosis can be quantified by the fluorescence intensity measured using flow cytometry.[41] The apoptotic population can be distinguished from the necrotic population with the addition of PI, which binds nucleic acids in cells only once the membrane becomes permeable (*i.e.* necrosis).

HSC cells were treated with 0.1 and 0.4 nM concentrations of peptide-conjugated gold nanoparticles and the percentages of apoptotic and necrotic cells were determined. The RGD/NLS-conjugated nanoparticles induce greater overall cell death than those conjugated with only RGD or only NLS (see Figure S4), which correlates well with the observed decrease in ATP for these nanoparticle formulations in particular. As shown in Figure 5, the AuNCs significantly induce more apoptosis (Fig. 5A) and necrosis (Fig. 5B) than the AuNSs. At higher treatment concentrations, the RGD/NLS-AuNCs induce apoptosis in HSC cells two times greater than RGD/NLS-AuNSs. At higher concentrations, the RGD/NLS-AuNCs induce thirty times more necrosis than RGD/NLS-AuNSs. It is also important to note that these nanoparticles induce minimal cell death in a control (HaCat) cell line (see Figure S6), as these cells do not overexpress alpha beta integrins[42] and thereby are not effectively targeted with the RGD conjugated nanoparticle. The drastic differences in which the peptide-conjugated nanoparticles, solid gold spheres and hollow gold cages, induce cell death in HSC cells prompt an explanation for how two different gold nanoparticle formulations could have such different effects on these cells.

Possible mechanism for enhanced nanoparticle-induced cell death by the nanocages

Since it has been shown previously that nanoparticle conjugates exhibit enhanced cellular effects compared to the free ligands in solution,[43, 44] we therefore propose that the RGD and NLS peptides conjugated to the nanoparticles are more effective than when free in solution. HSC cells were treated with the same concentration of NLS and RGD peptides as that which was added to the nanoparticles during conjugation (4 and 3.2 μM, respectively). The free NLS and RGD peptides induce much lower levels of apoptosis and necrosis, as seen in Figure 6, compared to that when conjugated to the AuNSs and AuNCs. This is possibly due to an RGD-dependent pathway. As was previously suggested by Salmon and coworkers, the RGD peptide activates pro-caspase-3, a pro-apoptotic protein, via interactions with an RGD-binding motif and subsequent conformational changes in the protein.[18, 19] It is possible that multivalency (*i.e.* localized RGD peptides bound to the gold nanoparticle surface) can enhance the overall effect of RGD on the cell.

Another mechanism is proposed based on the confirmation that the RGD/NLS-AuNCs reduce ATP and induce apoptosis and necrosis in HSC cells to a greater extent than RGD/NLS-AuNSs. As expected, based on the method of AuNC synthesis (see Experimental Procedures), ICP results show a 10% silver atom content in the metallic composition of the AuNCs used in this study (data not shown). Therefore, we consider the possibility that there could be Ag^+ ions present in the nanoparticle solution used for the treatment of HSC cells. In order to quantify the amount of Ag^+ ions, NaCl was added to the 0.4 nM RGD/NLS-AuNC solution, such that the NaCl concentration is slightly below its K_{sp}. Upon dissolution of NaCl in the 0.4 nM RGD/NLS-AuNC solution, no AgCl white precipitate was observed, indicating that the concentration of Ag^+ in the AuNC solution must be below 0.0456 nM. Therefore, HSC cells were treated with 0.0456 nM $AgNO_3$ to represent the maximum concentration of Ag^+ ions that could be present in the 0.4 nM RGD/NLS-AuNC treatment, as well as 10 and 20 nM $AgNO_3$, to represent the concentration of Ag^+ ions that would be needed in order to observe high levels of apoptosis or necrosis. Figure 6 displays the apoptotic and necrotic populations for cells treated with increasing concentrations of $AgNO_3$ (*i.e.* Ag^+ ions). It is obvious here that 0.0456 nM Ag^+ is not sufficient to induce apoptosis or necrosis to the extent at which the 0.4 nM RGD/NLS-AuNCs do. It is also apparent that the concentration of Ag^+ would have to be on the order of 20 nM for there to be significant apoptosis in HSC cells. Although the Ag^+ ions do not appear to induce apoptosis or necrosis, the residual silver atoms remaining on the inner cavity of the AuNCs could possibly have been oxidized in the cell culture medium to silver oxide (Ag_2O).[25, 45] To test this, AuNCs were left under physiological conditions, in cell culture medium, for 48 h, after which the

UV-Vis spectrum was taken in order to detect any changes in the surface plasmon resonance of the AuNCs. Indeed, a 51 nm redshift in the AuNC surface plasmon resonance was observed after 48 h in cell culture medium (see Figure S7), indicating the residual silver atoms on the inner cavity of the AuNC were oxidized to Ag_2O.[46-48] It has previously been shown, by Yen, *et. al.*,[25] that when Ag_2O is formed on the inside of the gold nanocage, it has the ability to produce hydroxyl radicals (generally termed reactive oxygen species (ROS)). These ROS have shown to damage DNA, ultimately leading to apoptosis, especially when located near the DNA,[26] as would be expected with the nuclear-targeted AuNPs studied here. Therefore, it is important to consider the possibility that ROS are generated by the RGD/NLS-AuNCs, which might be causing the observed enhanced apoptosis and necrosis[49] above that observed with RGD/NLS-AuNSs. Confocal imaging was performed to detect the presence of ROS in HSC cells treated with 0.4 nM RGD/NLS-AuNCs and AuNSs (Fig. 7). HSC cells were stained with H2DCFDA after treatment with nanoparticles and a green fluorescent (FITC) signal is generated when the acetate groups of H2DCFDA are removed during intracellular oxidation via the generation of ROS. The confocal images shown in Figure 7 show that there are indeed ROS in the RGD/NLS-AuNC-treated HSC cells, which is not seen with the RGD/NLS-AuNS treatment. The presence of ROS is also detected with other peptide-conjugated AuNCs, but not the AuNSs (see Figure S3). Although the ROS seen with the AuNCs is not as apparent as the ROS seen with a positive control (100 μM H_2O_2 for 3 h), it can still be concluded that the silver atom content on the innercavity of the AuNCs has an impact on the enhanced apoptosis and necrosis observed for the RGD/NLS-AuNC-treated HSC cells.

CONCLUSIONS

We have found here that hollow gold nanocages conjugated with nuclear targeting (NLS) and cancer cell penetration/pro-apoptotic (RGD) peptides induce apoptosis and necrosis in HSC cancer cells to a greater extent than solid gold nanospheres. The observed cell death is preceded by a number of different processes that also appear to be dependent on the concentration and shape/metallic composition of the peptide-conjugated gold nanoparticles. It is found that the 0.4 nM RGD/NLS-AuNCs and RGD/NLS-AuNSs induce cell cycle changes (*i.e.* G0/G1 phase accumulation, S phase depletion and G2/M phase depletion) (Fig. 3) and subsequently reduce ATP production in HSC cells (Fig. 4). The outcome of these cell cycle changes and reduction in ATP is apoptosis and necrosis (Fig. 5), with the greatest degrees of apoptosis and necrosis occurring when HSC cells are treated with the hollow gold nanocages. The increased apoptosis and necrosis seen with hollow gold nanocages can be explained based on the metallic composition of the gold nanocage. As a result of the synthesis, the gold nanocage has residual silver atoms on its inner cavity, which can be easily oxidized to Ag_2O, as observed by a redshift in the AuNC surface plasmon resonance (Fig. S7),[46-48] which in turn produces ROS,[25, 49] as observed by confocal microsopy of HSC cells treated with 0.4 nM RGD/NLS-AuNCs (Fig. 7). In conclusion, it is clear here that the metallic composition and thus, the shape of gold nanoparticles have an impact on their intrinsic antineoplastic properties, which can possibly be exploited further in the treatment of cancer.

Supplementary Material

Refer to Web version on PubMed Central for supplementary material.

Acknowledgments

The authors would like to acknowledge financial support provided by National Institutes of Health-National Cancer Institute grant U01CA151802-01.

REFERENCES

(1). Hirsch LR, Stafford RJ, Bankson JA, Sershen SR, Rivera B, Price RE, Hazle JD, Halas NJ, West JL. Nanoshell-mediated near-infrared thermal therapy of tumors under magnetic resonance guidance. Proceedings of the National Academy of Sciences of the United States of America. 2003; 100:13549–13554. [PubMed: 14597719]

(2). O'Neal DP, Hirsch LR, Halas NJ, Payne JD, West JL. Photo-thermal tumor ablation in mice using near infrared-absorbing nanoparticles. Cancer Lett. 2004; 209:171–176. [PubMed: 15159019]

(3). Dickerson EB, Dreaden EC, Huang XH, El-Sayed IH, Chu HH, Pushpanketh S, McDonald JF, El-Sayed MA. Gold nanorod assisted near-infrared plasmonic photothermal therapy (PPTT) of squamous cell carcinoma in mice. Cancer Lett. 2008; 269:57–66. [PubMed: 18541363]

(4). Huang XH, El-Sayed IH, Qian W, El-Sayed MA. Cancer cell imaging and photothermal therapy in the near-infrared region by using gold nanorods. J. Am. Chem. Soc. 2006; 128:2115–2120. [PubMed: 16464114]

(5). Huang XH, Jain PK, El-Sayed IH, El-Sayed MA. Gold nanoparticles: interesting optical properties and recent applications in cancer diagnostic and therapy. Nanomedicine. 2007; 2:681–693. [PubMed: 17976030]

(6). Chen JY, Wang DL, Xi JF, Au L, Siekkinen A, Warsen A, Li ZY, Zhang H, Xia Y, Li X. Immuno gold nanocages with tailored optical properties for targeted photothermal destruction of cancer cells. Nano Lett. 2007; 7:1318–1322. [PubMed: 17430005]

(7). El-Sayed IH, Huang XH, El-Sayed MA. Selective laser photo-thermal therapy of epithelial carcinoma using anti-EGFR antibody conjugated gold nanoparticles. Cancer Lett. 2006; 239:129–135. [PubMed: 16198049]

(8). Kang B, Mackey MA, El-Sayed MA. Nuclear Targeting of Gold Nanoparticles in Cancer Cells Induces DNA Damage, Causing Cytokinesis Arrest and Apoptosis. J. Am. Chem. Soc. 2010; 132:1517–1519. [PubMed: 20085324]

(9). Austin LA, Kang B, Yen CW, El-Sayed MA. Nuclear Targeted Silver Nanospheres Perturb the Cancer Cell Cycle Differently than Those of Nanogold. Bioconjugate Chem. 2011; 22:2324–2331.

(10). El-Sayed IH, Huang XH, El-Sayed MA. Surface plasmon resonance scattering and absorption of anti-EGFR antibody conjugated gold nanoparticles in cancer diagnostics: Applications in oral cancer. Nano Lett. 2005; 5:829–834. [PubMed: 15884879]

(11). Zitzmann S, Ehemann V, Schwab M. Arginine-glycine-aspartic acid (RGD)-peptide binds to both tumor and tumor-endothelial cells in vivo. Cancer Res. 2002; 62:5139–5143. [PubMed: 12234975]

(12). Xue H, Atakilit A, Zhu WM, Li XW, Ramos DM, Pytela R. Role of the alpha v beta 6 integrin in human oral squamous cell carcinoma growth in vivo and in vitro. Biochem. Biophys. Res. Commun. 2001; 288:610–618. [PubMed: 11676487]

(13). Xue H, Atakilit A, Zhu WM, Sheppard D, Ramos DM, Pytela R. Role of av beta 6 integrin in growth and migration of oral squamous cell carcinoma. Mol. Biol. Cell. 2000; 11:1363.

(14). Castel S, Pagan R, Mitjans F, Piulats J, Goodman S, Jonczyk A, Huber F, Vilaro S, Reina M. RGD peptides and monoclonal antibodies, antagonists of alpha(v)-integrin, enter the cells by independent endocytic pathways. Lab. Invest. 2001; 81:1615–1626. [PubMed: 11742032]

(15). Tkachenko AG, Xie H, Liu YL, Coleman D, Ryan J, Glomm WR, Shipton MK, Franzen S, Feldheim DL. Cellular trajectories of peptide-modified gold particle complexes: Comparison of nuclear localization signals and peptide transduction domains. Bioconjugate Chem. 2004; 15:482–490.

(16). Tkachenko AG, Xie H, Coleman D, Glomm W, Ryan J, Anderson MF, Franzen S, Feldheim DL. Multifunctional gold nanoparticle-peptide complexes for nuclear targeting. J. Am. Chem. Soc. 2003; 125:4700–4701. [PubMed: 12696875]

(17). Escriou V, Carriere M, Scherman D, Wils P. NLS bioconjugates for targeting therapeutic genes to the nucleus. Adv. Drug Delivery Rev. 2003; 55:295–306.

(18). Fischer U, Schulze-Osthoff K. Apoptosis-based therapies and drug targets. Cell Death Differ. 2005; 12:942–961. [PubMed: 15665817]

(19). Buckley CD, Pilling D, Henriquez NV, Parsonage G, Threlfall K, Scheel-Toellner D, Simmons DL, Akbar AN, Lord JM, Salmon M. RGD peptides induce apoptosis by direct caspase-3 activation. Nature. 1999; 397:534–539. [PubMed: 10028971]

(20). Huang XH, Kang B, Qian W, Mackey MA, Chen PC, Oyelere AK, El-Sayed IH, El-Sayed MA. Comparative study of photothermolysis of cancer cells with nuclear-targeted or cytoplasm-targeted gold nanospheres: continuous wave or pulsed lasers. J. Biomed. Opt. 2010; 15

(21). Oyelere AK, Chen PC, Huang XH, El-Sayed IH, El-Sayed MA. Peptide-conjugated gold nanorods for nuclear targeting. Bioconjugate Chem. 2007; 18:1490–1497.

(22). Chen JY, Wiley B, Li ZY, Campbell D, Saeki F, Cang H, Au L, Lee J, Li X, Xia Y. Gold nanocages: Engineering their structure for biomedical applications. Adv. Mater. 2005; 17:2255–2261.

(23). Cho EC, Au L, Zhang Q, Xio Y. The Effects of Size, Shape, and Surface Functional Group of Gold Nanostructures on Their Adsorption and Internalization by Cells. Small. 2010; 6:517–522. [PubMed: 20029850]

(24). Mahmoud MA, Snyder B, El-Sayed MA. Surface Plasmon Fields and Coupling in the Hollow Gold Nanoparticles and Surface-Enhanced Raman Spectroscopy. Theory and Experiment. J. Phys. Chem. C. 2010; 114:7436–7443.

(25). Yen CW, Mahmoud MA, El-Sayed MA. Photocatalysis in gold nanocage nanoreactors. J. Phys. Chem. A. 2009; 113:4340–4345. [PubMed: 19271721]

(26). Cadet J, Delatour T, Douki T, Gasparutto D, Pouget JP, Ravanat JL, Sauvaigo S. Hydroxyl radicals and DNA base damage. Mutat. Res. 1999; 424:9–21. [PubMed: 10064846]

(27). Siekkinen AR, McLellan JM, Chen JY, Xia YN. Rapid synthesis of small silver nanocubes by mediating polyol reduction with a trace amount of sodium sulfide or sodium hydrosulfide. Chem. Phys. Lett. 2006; 432:491–496. [PubMed: 18496589]

(28). Frens G. Controlled nucleation for regulation of particle-size in monodisperse gold suspensions. Nature (London), Phys. Sci. 1973; 241:20–22.

(29). Olenych SG, Moussallem MD, Salloum DS, Schlenoff JB, Keller TCS. Fibronectin and cell attachment to cell and protein resistant polyelectrolyte surfaces. Biomacromolecules. 2005; 6:3252–3258. [PubMed: 16283753]

(30). Liu XO, Atwater M, Wang JH, Huo Q. Extinction coefficient of gold nanoparticles with different sizes and different capping ligands. Colloids Surf., B. 2007; 58:3–7.

(31). Chithrani BD, Chan WCW. Elucidating the mechanism of cellular uptake and removal of protein-coated gold nanoparticles of different sizes and shapes. Nano Lett. 2007; 7:1542–1550. [PubMed: 17465586]

(32). Crouch SPM, Kozlowski R, Slater KJ, Fletcher J. The Use of Atp Bioluminescence as a Measure of Cell-Proliferation and Cytotoxicity. J. Immunol. Methods. 1993; 160:81–88. [PubMed: 7680699]

(33). Gao HJ, Shi WD, Freund LB. Mechanics of receptor-mediated endocytosis. P. Natl. Acad. Sci. U.S.A. 2005; 102:9469–9474.

(34). Feldherr CM, Akin D. The permeability of the nuclear-envelope in dividing and nondividing cell-cultures. J. Cell Biol. 1990; 111:1–8. [PubMed: 2365731]

(35). Feldherr CM, Akin D. Regulation of nuclear transport in proliferating and quiescent cells. Exp. Cell Res. 1993; 205:179–186. [PubMed: 8453991]

(36). Feldherr CM, Lanford RE, Akin D. Signal-mediated nuclear transport in simian-virus-40-transformed cells is regulated by large tumor-antigen. P. Natl. Acad. Sci. U.S.A. 1992; 89:11002–11005.

(37). Feldherr CM, Lanford RE, Akin D. Signal-mediated nuclear transport in simian-virus 40-transformed cells is regulated by large tumor-antigen. P. Natl. Acad. Sci. U.S.A. 1992; 89:11002–11005.

(38). Nakielny S, Dreyfuss G. Transport of proteins and RNAs in and out of the nucleus. Cell. 1999; 99:677–690. [PubMed: 10619422]

(39). Narayanan BA, Geoffroy O, Willingham MC, Re GG, Nixon DW. p53/p21(WAF1/CIP1) expression and its possible role in G1 arrest and apoptosis in ellagic acid treated cancer cells. Cancer Lett. 1999; 136:215–221. [PubMed: 10355751]

(40). Sweet S, Singh G. Accumulation of Human Promyelocytic Leukemic (Hl-60) Cells at 2 Energetic Cell-Cycle Checkpoints. Cancer Res. 1995; 55:5164–5167. [PubMed: 7585566]

(41). van Engeland M, Nieland LJW, Ramaekers FCS, Schutte B, Reutelingsperger CPM. Annexin V-affinity assay: A review on an apoptosis detection system based on phosphatidylserine exposure. Cytometry. 1998; 31:1–9. [PubMed: 9450519]

(42). Koivisto L, Larjava K, Hakkinen L, Uitto VJ, Heino J, Larjava H. Different integrins mediate cell spreading, haptotaxis and lateral migration of HaCaT keratinocytes on fibronectin. Cell Adhes. Commun. 1999; 7:245–257. [PubMed: 10626908]

(43). Tassa C, Duffner JL, Lewis TA, Weissleder R, Schreiber SL, Koehler AN, Shaw SY. Binding Affinity and Kinetic Analysis of Targeted Small Molecule-Modified Nanoparticles. Bioconjugate Chem. 2010; 21:14–19.

(44). Dreaden EC, Mwakwari SC, Sodji QH, Oyelere AK, El-Sayed MA. Tamoxifen-Poly(ethylene glycol)-Thiol Gold Nanoparticle Conjugates: Enhanced Potency and Selective Delivery for Breast Cancer Treatment. Bioconjugate Chem. 2009; 20:2247–2253.

(45). AshaRani PV, Low Kah Mun G, Hande MP, Valiyaveettil S. Cytotoxicity and genotoxicity of silver nanoparticles in human cells. ACS Nano. 2009; 3:279–290. [PubMed: 19236062]

(46). Yin YD, Li ZY, Zhong ZY, Gates B, Xia YN, Venkateswaran S. Synthesis and characterization of stable aqueous dispersions of silver nanoparticles through the Tollens process. J. Mater. Chem. 2002; 12:522–527.

(47). Kapoor S. Preparation, characterization, and surface modification of silver particles. Langmuir. 1998; 14:1021–1025.

(48). Chen M, Wang LY, Han JT, Zhang JY, Li ZY, Qian DJ. Preparation and study of polyacryamide-stabilized silver nanoparticles through a one-pot process. J. Phys. Chem. B. 2006; 110:11224–11231. [PubMed: 16771388]

(49). Moustafa MH, Sharma RK, Thornton J, Mascha E, Abdel-Hafez MA, Thomas AJ Jr. Agarwal A. Relationship between ROS production, apoptosis and DNA denaturation in spermatozoa from patients examined for infertility. Hum. Reprod. 2004; 19:129–138. [PubMed: 14688171]

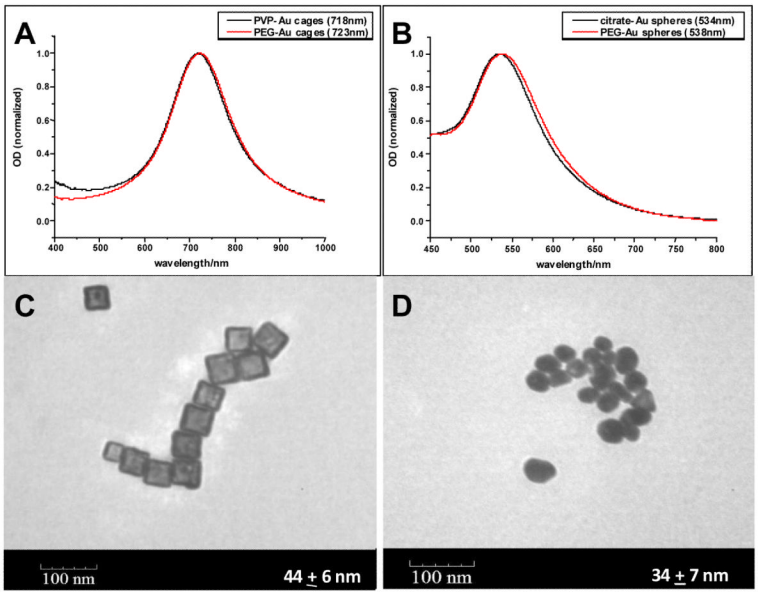

Figure 1.

UV-Vis absorption spectra of (A) PVP-AuNCs and (B) citrate-AuNSs before (black) and after (red) conjugation with PEG. Transmission electron micrograph of (C) 45 nm PVP-AuNCs and (D) 35 nm citrate-AuNSs.

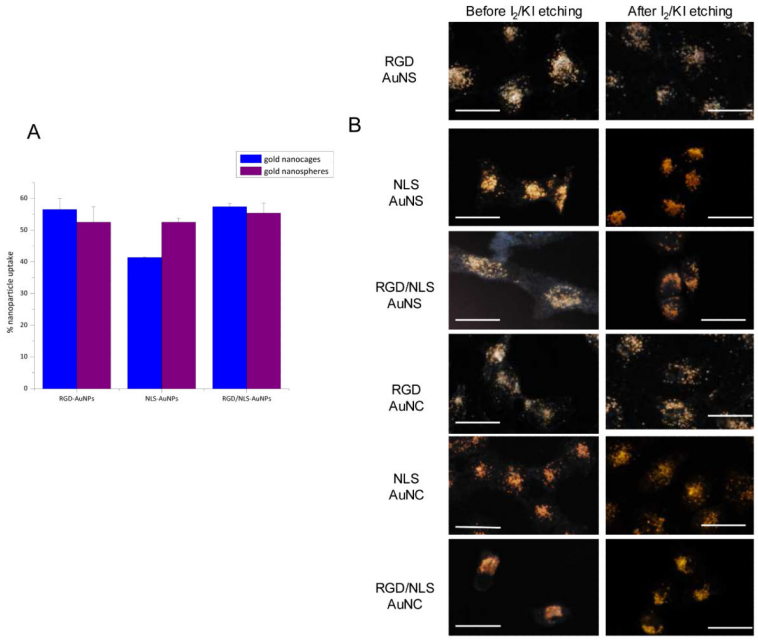

Figure 2.

Cellular internalization and nuclear localization of peptide-conjugated AuNPs by HSC cells after 48 h, determined as the percent uptake (A), as well as the with plasmonic dark field light scattering imaging (B) of internalized nanoparticles before and after etching of extracellular nanoparticles. Scale bar: 20 μm

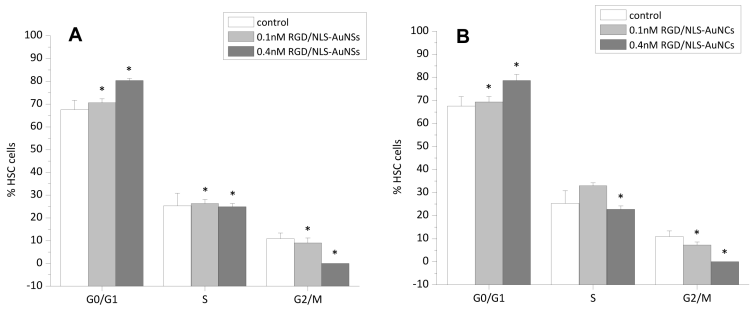

Figure 3.

Cell cycle changes induced by peptide-conjugated AuNPs, compared to control (HSC cells treated with nanoparticle-free culture medium). RGD/NLS-AuNSs (A), and RGD/NLS-AuNCs (B), at concentrations of 0.4 nM, both generate an increase in G0/G1 phase, a decrease in S phase and a decrease in G2/M phase populations when incubated with HSC cells for 48 h. Values expressed as mean ± standard deviation of three independent experiments. Statistical significance, with respect to control, indicated by * ($p < 0.05$).

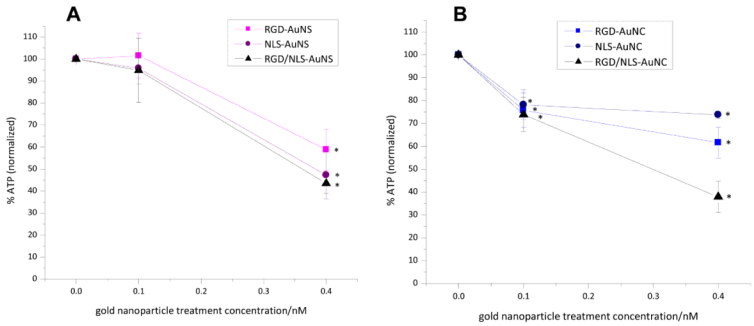

Figure 4.

ATP depletion induced by peptide-conjugated AuNPs (0.1 and 0.4 nM), normalized to the control (HSC cells treated with nanoparticle-free medium) after 48 h. The combination of RGD and NLS peptides conjugated to the nanoparticles allows for the greatest reduction in ATP in the case of the AuNSs (A) and AuNCs (B). Values expressed as mean ± standard deviation of three independent experiments. Statistical significance, with respect to control (0.0 nM), indicated by * ($p < 0.05$).

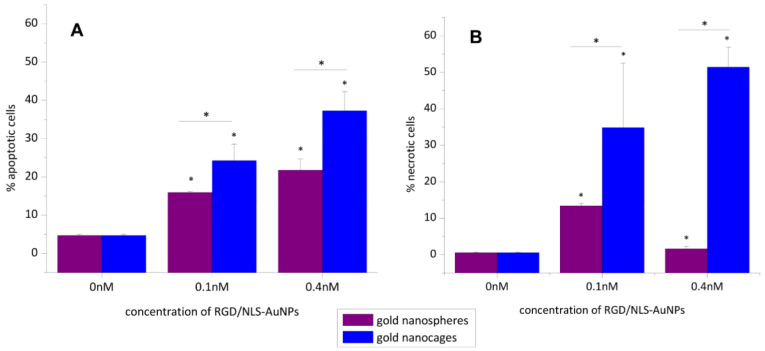

Figure 5.

Cell death, via apoptosis (A) and necrosis (B), induced in HSC cells after 48 h treatment with 0, 0.1, and 0.4 nM peptide-conjugated AuNSs (purple) and AuNCs (blue). The RGD/NLS-AuNCs, at 0.4 nM treatment concentrations, induce the greatest amount of cell death. Values expressed as mean ± standard deviation of three independent experiments. Statistical significance, with respect to control (above each bar) and between AuNSs and AuNSs (above each line) indicated by * ($p < 0.05$).

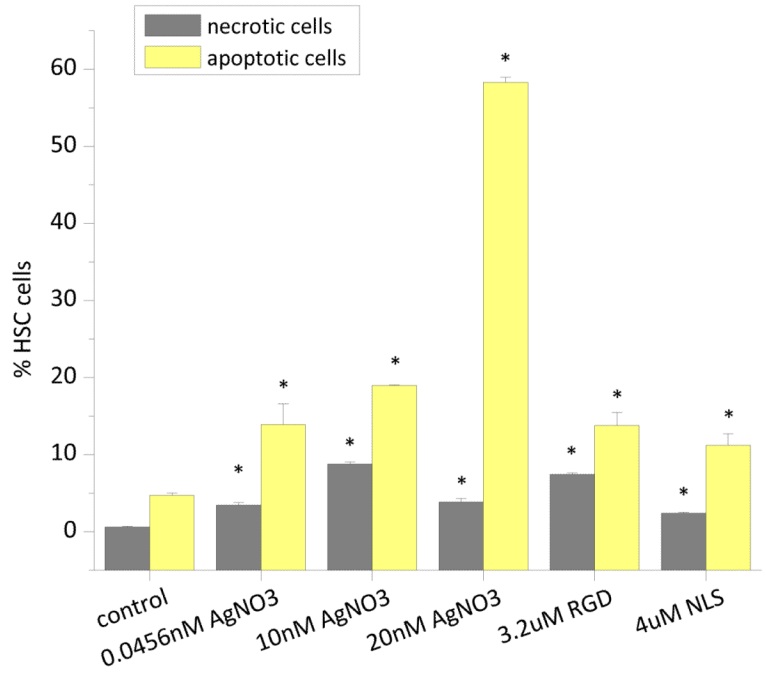

Figure 6.

Cell death induced, via apoptosis (yellow) and necrosis (grey), in HSC cells after 48 h treatment with varying concentrations $AgNO_3$ (*i.e.* Ag^+ ions), as well as free peptides in culture medium (3.2 μM RGD and 4 μM NLS). Values expressed as mean ± standard deviation of three independent experiments. Statistical significance, with respect to control, indicated by * ($p < 0.05$).

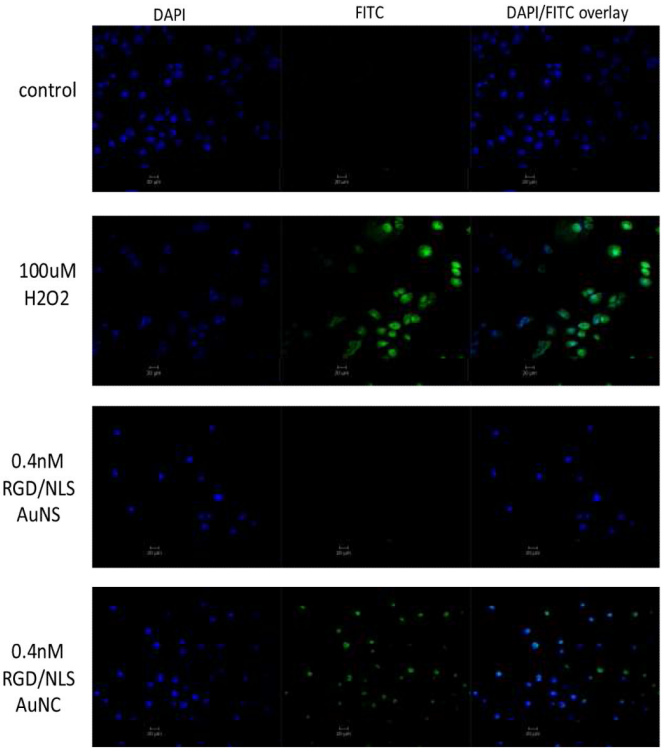

Figure 7.

Reactive oxygen species (ROS) generation detected by confocal microscopy for 0.4 nM RGD/NLS-AuNSs and AuNCs. DAPI panel (left) shows the nuclei of HSC cells stained blue. FITC panel (middle) represents green fluorescence indicative of ROS generated inside cells. DAPI/FITC overlay (right) shows the combination of both nuclei and ROS. Control (cells treated with nanoparticle-free medium) exhibits minimal FITC fluorescence, along with the 0.4 nM RGD/NLS-AuNSs. 100 μM H_2O_2 shows high FITC fluorescence, used as a positive control for ROS generation. The 0.4 nM RGD/NLS-AuNCs display FITC fluorescence, indicating ROS are generated in HSC cells with this nanoparticle treatment. Scale bar: 20 μm.